IEEE Open Journal of
Ultrasonics, Ferroelectrics, and Frequency Control

Received 10 June 2022; accepted 1 August 2022. Date of publication 16 August 2022; date of current version 25 August 2022.

Digital Object Identifier 10.1109/OJUFFC.2022.3197104

Thermal-Mechanical Noise Modeling and Measurements of a Row-Column Addressed CMUT Probe

TONY MERRIEN[1,2], AUDREN BOULMÉ[2], AND DOMINIQUE CERTON[1] (Member, IEEE)

[1]GREMAN UMR 7347, CNRS, INSA Centre Val de Loire, University of Tours, 37100 Tours, France
[2]MODULEUS SAS, 37100 Tours, France

CORRESPONDING AUTHOR: D. CERTON (dominique.certon@univ-tours.fr)

ABSTRACT Thermal-Mechanical (T-M) noise is a natural phenomenon occurring in Capacitive Micromachined Ultrasonic Transducers (CMUT). T-M noise is a value of great interest because it is linked to the minimal detectable pressure of a transducer and can also serve as a convenient characterization tool. Indeed, the general behavior of a CMUT array is translated through its T-M noise which does not require any external applied source to be assessed. However, T-M noise is difficult to measure, often time requires a dedicated measurement chain and is mostly based on spectrum analyzers in a carefully controlled environment. In this paper, we present a temporal technique to characterize the T-M noise of CMUT-based arrays with a commercially available amplifier and a digital oscilloscope. The approach is applied to an air coupled Row-Column Addressed (RCA) matrix array, for which the elements cannot be measured with traditional microprobes systems. This task is performed using a Printed Circuit Board (PCB) dedicated to the characterization of RCA arrays and designed to drive rows and columns individually. Noise Power Spectral Density (PSD) modeling of the complete measurement chain is achieved using a lumped-parameter model of the RCA array element and using the amplifier gain, electrical impedance, and noise characteristics. Measurements obtained with the signal analyzer and the temporal method are in good agreement with the model. The presented characterization technique can be extended to other micromachined ultrasonic transducer probe architectures, technologies, and amplification systems.

INDEX TERMS Capacitive, micromachined, MEMS, RCA, electronics, characterization, modeling, cross-spectrum.

I. INTRODUCTION

SINCE the discovery of thermal noise by Johnson and Nyquist [1], [2], its effects has been extensively studied for Micro-Electro-Mechanical Systems (MEMS) [3]. In the case of ultrasonic transducers, noise assessment is a very valuable information since it provides the lower limit of detectable pressure [4]. This sets the value at which the measurement chain will no longer be able to translate information originating from the medium reliably. The commonly employed terminology, Thermal-Mechanical (T-M) noise, translates two analogous physical noise phenomena [5]. On one hand, thermal noise arises from the Brownian motion of electrons inside any resistive system at equilibrium and produces a slight random electrical potential variation. On the other hand, mechanical noise arises from the Brownian motion of molecules inside any damped system at equilibrium and produces a slight random displacement potential. Other electrical noise sources exist in conductors such as shot noise due to transport quantization of charges at non-equilibrium states [6] or flicker (*i.e.*, $1/f$) noise related to resistance fluctuations mostly at low frequencies [7]. Because Capacitive Micromachined Ultrasonic Transducer (CMUT) arrays output noise was proven to be dominated by T-M noise [8], these other noise sources will not be discussed in this paper.

A CMUT is a sensor based on a capacitor architecture, with a fixed and a moving electrode actuated by electrostatic forces [9], [10]. CMUT applications range from volatile organic compounds detection, to medical therapy and ultrasound imaging [11]. T-M noise is an intrinsic phenomenon occurring in CMUTs [12]–[14]. However, T-M noise in CMUT arrays is generally low compared to the

noise contribution of other components in the measurement chain. Therefore, it poses major measurement challenges and generally requires dedicated electronics monolithically integrated with a specific transducer. For instance, Gurun *et al.* were able to measure CMUT T-M noise using a monolithically integrated CMOS Application-Specific Integrated Circuit (ASIC) comprised of a low-noise transimpedance amplifier (TIA) [8], [15]. If this result demonstrates the measurement feasibility of T-M noise, the protocol generalization towards CMUT arrays based on hybrid electronic integration architectures is limited.

The first objective of this paper is to show that the noise of a CMUT probe based on a hybrid electronic architecture can be modeled. Hybrid electronic integration architectures are the most versatile approach to associate CMUT arrays with dedicated embedded driving electronics. It consists in a specific chip or circuit designed for each electronic function required to perform operations with an ultrasound probe. All the functions are then gathered in one or multiple PCBs (Printed Circuit Boards) and packaged in the ultrasonic probe head. This approach allows the CMUT array and the electronics to be designed, fabricated and optimized separately before flip-chip bonding [16]. The electronic driving circuits may also be separated from the probe head. Noise modeling of the CMUT and its electronics assembly is difficult because the PCB architecture as well as the noise characteristics of the preamplification circuits used need to be considered. Moreover, T-M noise assessment is generally performed on spectrum analyzers which may require a specific calibration process and limit the fast and easy access to noise results, hence transducer properties.

The second objective is to show that T-M noise can be measured using a digital oscilloscope combined with a frequential post-processing cross-correlation approach. The frequential cross-correlation technique (also called ''cross-spectrum'') used in this paper has been thoroughly described in great details by Rubiola and Vernotte [17]. Practical applications of signal cross-correlation extend beyond the scope of this paper and has been used in multiple other scientific domains, ranging from geophysics [18] to ultrasound imaging [19]. Two different measurement protocols will be implemented and used to validate the proposed modeling approach.

This work is focused on a Row-Column Addressed (RCA) CMUT-based probe whose architecture is particularly critical and intricate compared to a conventional linear array [20]. Recently, several CMUT arrays architectures have emerged to address 3-D imaging needs, and amongst them RCA matrices. For this purpose, our group has developed a first generation of RCA CMUT arrays comprised of $64 + 64$ elements fabricated by wafer-bonding [21] on a borosilicate glass substrate to naturally eliminates parasitic capacitive coupling [22]. Rows and columns of a RCA array cannot be addressed natively in the same manner as 1-D linear arrays using standard micro-probes. To imitate orthogonal 1-D arrays, a common ground needs to be applied on rows or columns [23]. Our interest lies within full rows and columns driving conditions, which enable synthetic aperture [24] and plane wave imaging [19]. Motivated by this background, this paper aims to model and measure T-M noise of an air coupled RCA CMUT probe. However, noise modeling of an array comprised of hundreds of cells can be tedious [25]. We will show that the two-port network model of a CMUT array element recently published by our group simplifies the noise modeling [26].

The first section describes the lumped-parameter CMUT model of the RCA array element used. Parasitic components are introduced with great care and the interface electronics used to drive the RCA array is described. Model validation is achieved through an electrical admittance measurement comparison. The second section introduces the amplifier in the model based on its characteristics. The amplifier equivalent associated voltage and current noises are measured using a signal analyzer. This allows us to model a complete T-M noise measurement chain. The third section describes the measurement acquisition equipment, principles and results obtained with the two different experimental methods. First, a temporal approach is used with a digital oscilloscope and a general-purpose, commercially available, current amplifier. The measurements are then post processed using signal cross-correlation to retrieve the T-M noise information. Then, using the same amplifier, measurements are performed on a spectrum analyzer. Note that throughout this paper, measurements and modeling are performed in air with an emphasis on current noise. Indeed, our RCA CMUT device was designed for low impedance current driven applications. Nevertheless, the measurement protocols presented here can be extended to other voltage driven arrays architectures and high impedance voltage amplifiers.

II. CMUT NOISE MODELING

This section describes the noise modeling of a bare CMUT chip by considering the electrical interconnection scheme. The RCA array prototype as well as the driving PCB used to validate simulation results are described. Then, to ensure the model input parameters validity, a comparison with experimental electrical impedance measurements is performed.

A. CMUT NOISE WITH PARASITIC COMPONENTS

For the remaining sections of this paper, the term ''element'' will be used to describe a full row or column of the RCA matrix. The design parameters of the RCA CMUT array made of square shaped cells used in this study are presented Table 1. The membranes are made of a silicon layer fully covered with an aluminum electrode (cf. Fig. 2). The gap thickness was designed to obtain a low collapse voltage and drive the array with voltages as low as $20V$. This type of array is intended for low-power consumption ultrasound systems.

The modeling approach is based on the finite-difference, multiscale method developed by Meynier *et al.* [27] and recently extended to an equivalent two-port network representation of the array element by Merrien *et al.* [26]. The lumped-parameter approach of the array element enables the combination of hundreds of cells into single equivalent

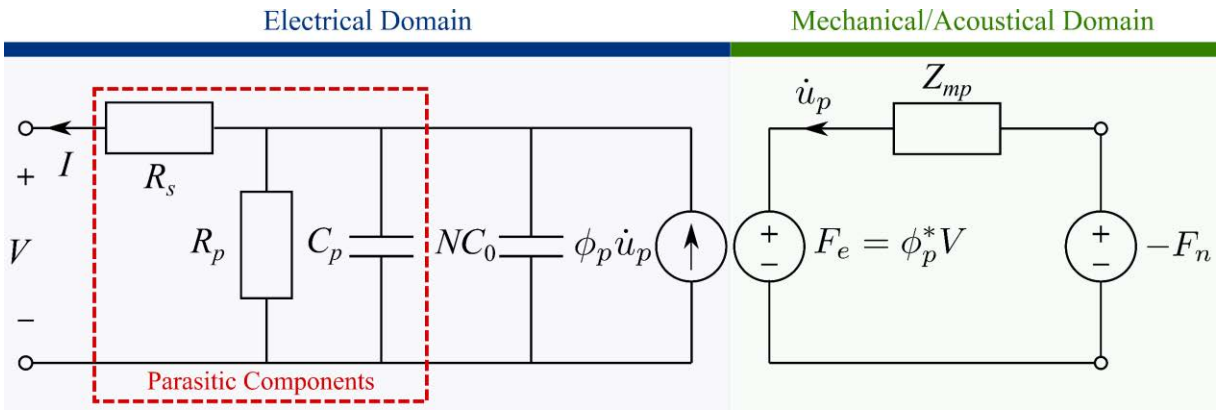

FIGURE 1. Electroacoustic equivalent circuit of a CMUT array element in air and in receive mode. Additional parasitic components linked to the properties and the geometry of the materials used is highlighted in the dashed red box.

TABLE 1. RCA CMUT array design parameters.

Design parameter	Value
CMUT cell	
Side length (square)	26 μm
Distance between cells	3 μm
Vacuum gap height	60 nm
Measured collapse voltage	22 V
Array	
Number of elements	64 + 64
Cells per element	9
Element width	94 μm
Element length	94 μm
Element kerf	5 μm
Element pitch	99 μm

TABLE 2. Description of the lumped-parameters used in the equivalent circuit model of the RCA CMUT array element in receive mode.

Lumped-parameter	Definition
Z_{mp}	Mechanical impedance
C_0	Static capacitance
C_p	Parasitic capacitance
R_p	Dielectric losses
R_s	Resistive losses
ϕ_p	Transformation coefficient
F_e	Electroacoustic force
V	Output voltage
I	Output current
$\dot{u}_p$	Input membrane velocity
F_n	Input acoustic force

impedance terms, hence easier implementation of parasitic components and integration of cascaded two-port networks. The lumped-parameters associated with the equivalent circuit model of a RCA CMUT array element in receive mode are presented Table 2. The array element is comprised of $N = 576$ cells, hence its total static capacitance is $NC_0 = 44pF$ at $V_{DC} = 0.8V_c$. The lumped-parameter CMUT array element equivalent circuit is presented Fig. 1. The force associated to the noise input F_n is negative because of the chosen convention to represent the array element in receive mode [26].

To consider the complete electrical behavior of the array, one can use additional components such as a parallel parasitic capacitance C_p, a parallel impedance R_p to account for dielectric losses and a series resistance R_s to model the resistive losses linked to the electrodes. The parasitic components presented here are associated to the bare RCA dice only sketched Fig. 2. The parasitic capacitance is a value linked to the inactive electrode surface S_a of the array element and the equivalent gap size h_{heq}

$$C_p = \frac{\varepsilon_0 S_a}{h_{eq}} \tag{1}$$

where $\varepsilon_0 = 8.85 \times 10^{-12} F/m$ is the vacuum dielectric permittivity. Parasitic capacitance has been widely discussed and was shown to reduce the effective coupling coefficient [28] as well as the overall integrated system performance [16]. Hence, this parasitic component needs careful attention while designing CMUTs. The proposed design in this paper leads to $C_p = 33.5pF$ for each array element. At $V_{DC} = 0.8V_C$, the parasitic capacitance can be expressed as a function of the static capacitance of the element such that $C_p = 0.76NC_0$.

Classically, dielectric losses can be expressed through the loss angle δ of the insulation layer [29] through a parallel impedance term equal to

$$R_p = \frac{1}{\omega \left(NC_0 + C_p\right) \tan\left(\delta\right)} \tag{2}$$

The loss angle is material dependent, based on the dielectric insulation used. Here, the loss angle is set to silicon dioxide (SiO_2) accordingly, which is the insulation material used for the CMUT design, with $\delta = 0.001$ [30]. Note that the dielectric losses may have prominent effects in the low frequency range. Our device possesses a resonant frequency that is near

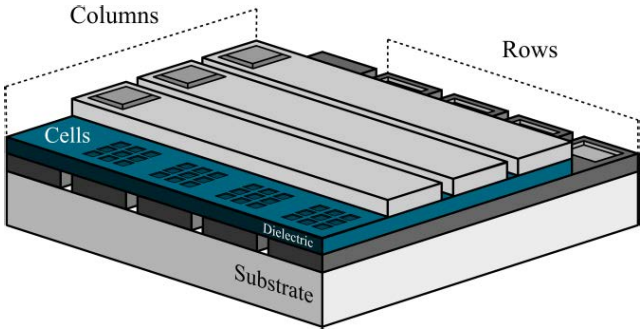

FIGURE 2. Sketch of a RCA CMUT array portion. Based on the fabricated device, the top electrodes constitute the column elements (which are fully metallized), while the bottom electrodes constitute the row elements. The inactive surface S_a is the total space in-between cells within an element.

$15MHz$ while in air, hence dielectric losses effects are almost negligeable.

Finally, the resistive losses due to the electrode resistance depend on the geometry of the overall array and the properties of the material used. As detailed by Havreland *et al.* [31], resistive losses are linked to intricate relationships between cells among the element and can have a detrimental effect on the array performance. Through a parameter fit of an electrical impedance measurement using our RCA CMUT device (cf. Fig. 5 in the next section), the resistive losses can be approximated by an equivalent scalar series resistance of $R_s = 20\ \Omega$. The results presented in this paper are focused on column elements accessed through the top electrode. Other RCA devices may have opposite row/column and top/bottom architectures [32]. The impedance equation Z_{elec} associated with this complete CMUT array element model in air can be expressed as

$$Z_{elec} = \left[j\omega \left(NC_0 + C_p \right) + \frac{1}{R_p} + \frac{\left|\phi_p\right|^2}{Z_{mp}} \right]^{-1} + R_s \qquad (3)$$

The expression of electrical impedance (or admittance) is the key components to electrical noise assessment. Indeed, the common noise equations of an electrical system are called Johnson-Nyquist relations and are expressed through a statistical variance. This variance can be related to a spectral distribution, commonly described by a Power Spectral Density (PSD) [33]. PSD of noise are expressed in V^2/Hz for a noise voltage and in A^2/Hz for a noise current, which gives respectively

$$\begin{cases} \bar{v_b^2} = 4k_bT\Re\left(Z_{elec}\right) \\ \bar{i_b^2} = 4k_bT\Re\left(Y_{elec}\right) \end{cases} \qquad (4)$$

Here, Y_{elec} is the electrical admittance of the device under test, $k_b = 1.38 \times 10^{-23} kg.m^2/s^2/K$ is the Boltzmann constant, and T is the temperature. The temperature is kept constant throughout this paper at an ambient $T = 290K$. Parasitic components introduced in the CMUT model influence its T-M noise. Results of a CMUT array element T-M noise based on equations (3) and (4) are plotted Fig. 3 with and without parasitic components. In this section, modeling and measurements are performed using a biasing of $V_{DC} = 0.8V_C$, which is a classical value for ultrasound imaging applications that also satisfies here a low driving voltage criterion of less than $20V$.

Results from Fig. 3 demonstrate the importance of parasitic components assessment during CMUT array design. As explained in the introduction, the remaining sections of the paper will be focused on the noise sensed through a current amplifier (*i.e.*, the noise source presented Fig. 3(b)). If not carefully addressed, parasitic components associated with the CMUT array design may not reveal clear resonances. It is apparent on these simulations that parasitic components may also increase the overall CMUT T-M noise hence deteriorate the minimal detectable pressure and affect the overall performances of the device.

B. ELECTRICAL IMPEDANCE MEASUREMENTS

In a probe head, CMUT arrays are mounted on a specific PCB which enables each element to be driven individually and to be connected to an electronic driving circuit board. Here, a specific PCB was designed to perform such task for all rows and columns of the RCA matrix. A single switch is assigned to each element with the possibility to connect them to the ground of the PCB or an output SMA connector. The CMUT array elements were wire-bonded on the PCB, protected by a glop-top layer, and connected to individual switches to drive the elements. Connectors with RC decoupling components (a $100nF$ capacitance and a $100k\Omega$ resistor) enable the distribution of polarization on one hand and output voltage sensing one the other hand. A sketch and a photography of the monolithic device is presented Fig. 4.

To ensure the validity of the approach and the relevance of the parasitic components accounted for in the model, electrical admittance measurements of a RCA CMUT integrated on the PCB were performed using a 4294A impedance analyzer (Agilent Technologies Inc., Santa Clara, CA, USA). The modulus of the electrical admittance measured is compared with the model results, as presented Fig. 5.

Modeling and measurement display the same overall behavior with an accurate depiction of resonant frequencies. On one hand, this translates the general accuracy of the model and the parasitic values of the array accounted for. On the other hand, the measurement was made possible using the dedicated PCB which is revealed to be suitable for RCA array characterization. Measurements and simulation results for frequencies higher than the anti-resonance slightly diverge even when accounting for the parasitic components of the array. We suspect this phenomenon to be linked to the RCA dedicated PCB used that may affect the measurements. Indeed, the electrical wires length and the additional components on the PCB presented Fig. 4 (*e.g.*, switches) are not accounted for in the model.

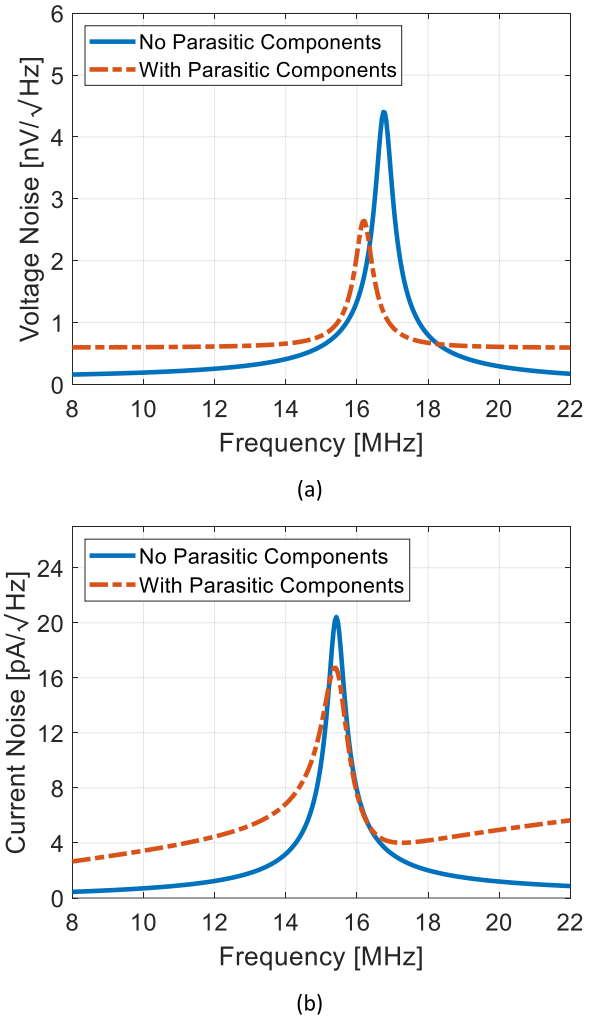

FIGURE 3. **(a) Voltage and (b) current noise results obtained for the CMUT array element with the lumped-parameter model with and without parasitic components at $V_{DC} = 0.8V_C$ and $T = 290K$.**

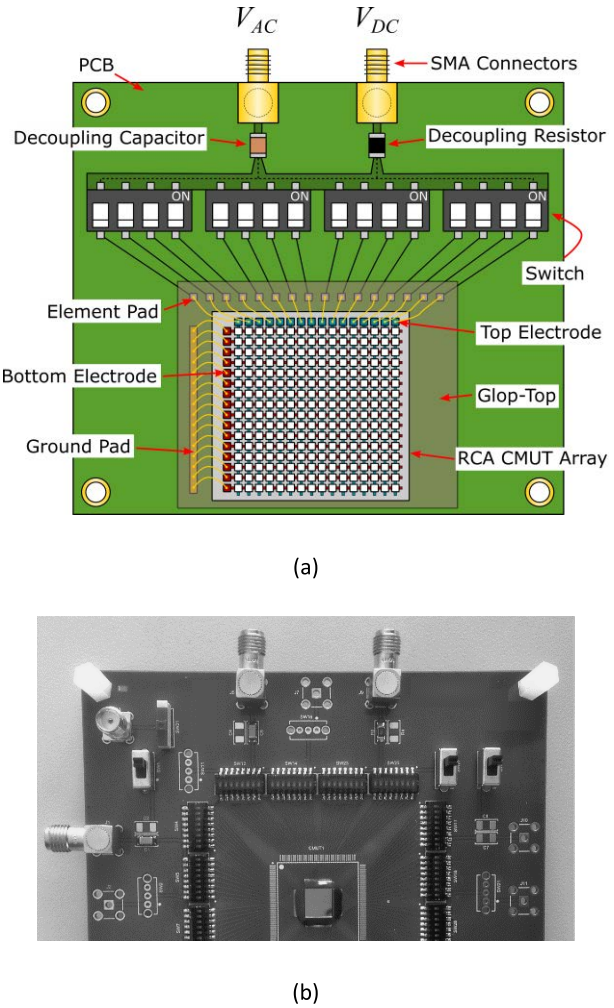

FIGURE 4. **(a) Sketch and (b) photography of the integrated probe used to perform RCA element measurements. The CMUT array elements are wire-bonded to the PCB pads and wires are protected by a glop-top layer. Each switch enables single CMUT element driving. Sensing and polarization are achieved with two different connectors and RC decoupling components.**

III. NOISE MODELING WITH AN AMPLIFIER

This section introduces the amplifier into the model. To assess properly its noise contribution and account for its presence accurately, the evaluation of the amplifier characteristics in the frequency domain of interest was performed. Modeling results of the complete instrumentation chain are presented.

A. AMPLIFIER CHARACTERISTICS

To set the noise level of the device under test above the acquisition equipment noise floor, the common solution is to use a low noise amplifier. In this study, we used the commercially available transimpedance amplifier HCA-100M-50K-C (Femto Messtechnik GmbH, Berlin, Germany) that possesses, based on the manufacturer datasheet, a bandwidth of $100MHz$ and a transimpedance gain of $G = 5 \times 10^4 V/A$ using a 50Ω electrical load. Note that the high capacitance of the RCA CMUT will degrade the amplifier bandwidth performance, a behavior which needs to be accounted for. The amplifier possesses a 50Ω output impedance, ideal for coaxial cable connection and other equipment with matched impedance. To model the noise generated by an amplifier, the classical approach is to use equivalent open current i_n and short voltage e_n noise sources as inputs of a noiseless gain stage. The equivalent circuit model of the complete measurement chain is presented Fig. 6.

To assess the gain of this specific system comprised of a CMUT and a current amplifier, one needs to know the CMUT array element electrical impedance (cf. equation (3)) as well as the amplifier input impedance. For instance, as provided by the current amplifier datasheet, its equivalent input impedance Z_{amp} consists of a 56Ω resistance in parallel with a $5pF$ capacitor. This means that the overall transfer function of the given system G_{sys} is comprised of the two cascaded impedances previously described and is equal to

$$G_{sys} = \frac{GZ_{elec}}{Z_{amp} + Z_{elec}} \tag{5}$$

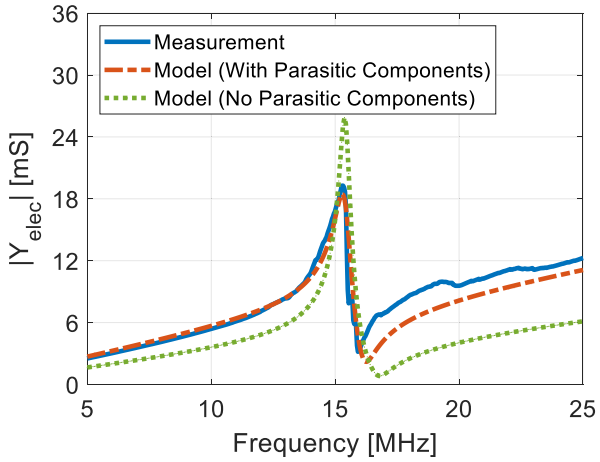

FIGURE 5. **Modulus of the electrical admittance measured and modeled in the air of the RCA CMUT array element integrated on a PCB for $V_{DC} = 0.8V_C$.**

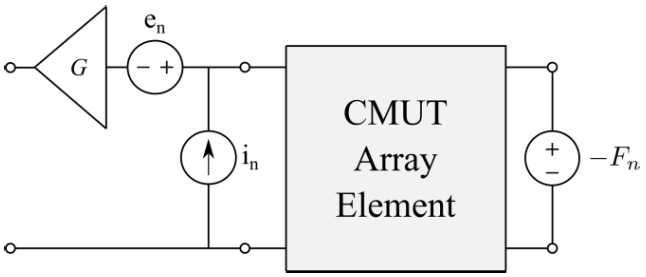

FIGURE 6. **Electrical equivalent circuit model of a measurement chain comprised of a CMUT array element and its parasitic components as well as an ideal noiseless amplifier with two equivalent input noise sources.**

The transfer function of the system for different CMUT bias voltages is plotted Fig. 7.

The variation of impedance as a function of frequency and the bias voltage of the CMUT element is translated as expected on the transfer function of the overall system. The results show that the transimpedance gain of $G = 5 \times 10^4 V/A$ decreases as the frequency increases. Indeed, this is due to the impedance mismatch between the amplifier input and the CMUT array. This result is key for optimal amplifier design and integration depending on each array design. The ideal amplification gain is obtained here when the impedance of the connected device is very high compared to the amplifier input impedance (*i.e.*, $Z_{elec} \gg Z_{amp}$).

The PSD of the measurement chain total noise output $\overline{V_{out}^2}$ comprised of a current amplifier with equivalent current and voltage noise sources can be expressed as [34]

$$\overline{V_{out}^2} = |G_{sys}|^2 \left(4k_bT\Re\left(Y_{elec}\right) + \overline{i_n^2} + \overline{e_n^2}\,|Y_{elec}|^2\right) \quad (6)$$

Note that even if the current of the device under test is sensed through the amplifier, the transimpedance gain translates a voltage at the amplifier output. In the remaining sections of this paper, we denote the output noise voltage to be the noise current of the system after the transimpedance gain stage. Here, one can see the contribution of the electrical

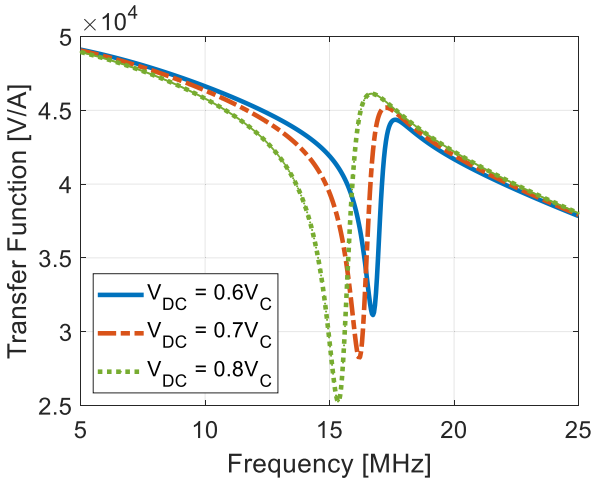

FIGURE 7. **Transfer function of the instrumentation chain comprised of a current amplifier and a RCA CMUT element for different bias voltages as a function of frequency.**

admittance of the CMUT through the voltage noise source of the amplifier. Note that an analogous expression exists for a voltage preamplifier using the electrical impedance expression of the device [35]. To model accurately the noise of the complete measurement chain, knowledge of the equivalent noise sources is mandatory.

To measure the noise characteristics of the preamplifier, a signal analyzer N9010A (Keysight Technologies, Santa Rosa, CA, USA) was used. On one hand, the measurement of the short voltage noise source e_n requires the input of the amplifier to be shorted to bypass the equivalent noise current source depicted Fig. 6. On the other hand, the measurement of the open current noise source i_n requires the input of the amplifier to be opened to bypass the equivalent noise voltage source depicted Fig. 6. The measured amplitude spectral density of the two equivalent input noise sources are plotted Fig. 8. The resolution bandwidth (RBW) used to make the measurement was set at $30kHz$. Moreover, to move the measured noise sources PSD at the preamplifier input, the gain value used was set to the datasheet value (*i.e.*, $5 \times 10^4 A/V$).

These results are close to the manufacturer provided values (*i.e.*, $\sqrt{\overline{e_n^2}} = 0.9nV/\sqrt{Hz}$ and $\sqrt{\overline{i_n^2}} = 3.8\ \text{pA}/\sqrt{Hz}$ at $10MHz$). The characterization process of the amplifier is mandatory to isolate the device noise from the complete measurement chain result. Careful attention should be paid to the system gain since its value depends on the electrical impedance of the device connected and used as a source, hence may vary for other CMUT devices. For this reason, T-M noise assessment could benefit from a voltage amplifier since a CMUT array element impedance is more likely to be negligible regarding their high input impedances.

B. NOISE MODELING OF THE COMPLETE INSTRUMENTATION CHAIN

Now that every variable is known, the total noise of the measurement chain comprised of a RCA CMUT array element

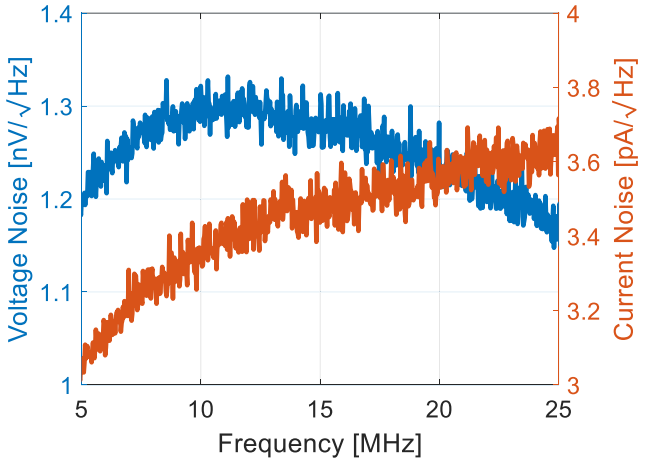

FIGURE 8. **Measurement of the equivalent voltage and current amplitude spectral density noise sources of the current amplifier using a signal analyzer at a resolution bandwidth of 30 kHz.**

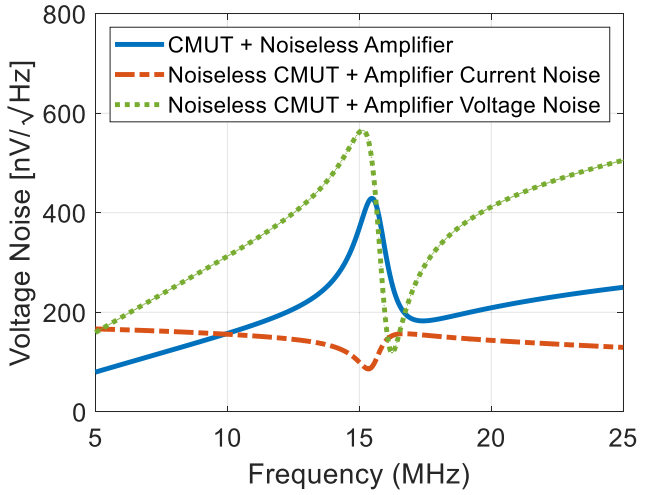

FIGURE 9. **Simulations of each individual noise source of the complete measurement chain using a bias voltage of $V_{DC} = 0.8V_C$.**

and a transimpedance amplifier can be modelled. For simplicity, only the mean contribution of the equivalent sources of the current amplifier in the frequency range of interest were considered in the model (*i.e.*, $\sqrt{\overline{e_n^2}} = 1.25nV/\sqrt{Hz}$ and $\sqrt{\overline{i_n^2}} = 3.45pA/\sqrt{Hz}$). Based on equation (6), the different noise sources of the measurement chain can be separately evaluated. For instance, Fig. 9 represents the noise of the CMUT with the noiseless amplifier, the equivalent current noise of the amplifier noise and the equivalent voltage noise of the amplifier (*i.e.*, each of the individual noise source terms of equation (6)). All the results are obtained using the gain G_{sys}.

This result shows that the main noise source is the equivalent noise voltage of the current amplifier which is translated here through the absolute admittance of the CMUT device. The CMUT noise combined with the noiseless amplifier reflects the noise of the isolated CMUT, as presented previously Fig. 3. The global noise voltage of the measurement chain comprised of all these noise sources is simulated and presented Fig. 10 for different biasing voltages.

Modeling results show that the CMUT behavior is still translated through the spring softening effect as the bias voltage increases. Therefore, noise measurement remains an ideal characterization tool for the assessment of CMUT properties even when using this type of amplifier. Modeling also shows that the noise levels reached here are superior to a general-purpose acquisition equipment input channel (*e.g.*, signal analyzer, oscilloscope) and therefore ensures the measurements feasibility. Furthermore, it allows for a fast and easy access to the general behavior of the measurement chain which can be used to tweak global parameters, choose the adequate measurement equipment, design CMUT arrays and more. Note that additional two-port network systems could be cascaded within the equivalent circuit model if other components needed to be added in the measurement chain (*e.g.*, cables). This modeling approach enables easier integration of each component of a full ultrasound acquisition system.

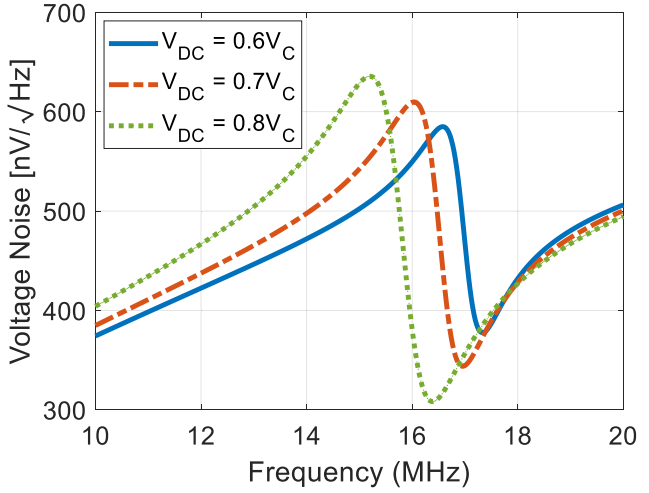

FIGURE 10. **Noise modeling of the complete measurement chain comprised of a RCA CMUT array element and a current amplifier for different bias voltages.**

IV. CMUT NOISE MEASUREMENTS

This last section focuses on the noise measurement of the whole instrumentation chain made of the RCA CMUT mounted on the PCB board followed with the amplification circuit. As proposed in the introduction, two measurement methods of the noise PSD were implemented and tested. One using a frequential approach with a signal analyzer and one based on a temporal approach using a digital oscilloscope, the latter being described first.

A. AUTO- AND CROSS-CORRELATION APPROACHES

The PSD measurement of a given source named here $c(t)$ can be obtained by means of a digital oscilloscope, provided that the noise is ergodic. Several successive acquisitions of the noise $c(t)$ enable computation of the PSD by averaging the set of energy spectral density $\langle C(f) \rangle$ obtained for each

realization such that

$$\langle S_{cc}(f)\rangle_m = \frac{1}{T}\langle |C(f)|^2\rangle_m \tag{7}$$

where m is the acquisition number and T is the finite time over which the acquisition was performed. Here, $C(f)$ is the Fourier transform of $c(t)$, hence the auto-correlation function. The main limitation of this approach remains in the noise level arising from the oscilloscope itself, which contains instrumentation noise (*e.g.*, cabling, oscilloscope probe) and quantization noise. If the acquisition channel is noisier than the device under test, the PSD of the noise obtained corresponds to the acquisition channel and not to the device itself.

Another technique, more suitable for noise evaluation through a temporal-based method, is the cross-correlation function of two different partially correlated signals denoted $x(t) = a(t)+c(t)$ and $y(t) = b(t)+c(t)$, obtained with two different acquisition chains. Here, $a(t)$ and $b(t)$ are noise signals linked to the two acquisition chains, assumed to be uncorrelated. We summarized the basic principle of this method in the appendix of this paper for completeness. Theoretically, the multiplication of two uncorrelated noise spectra averaged over a large enough number of acquisitions m tends towards zero [17]. Therefore, the cross-spectrum of these two partially correlated signals leads to

$$\langle S_{xy}(f)\rangle_m = \frac{1}{T}\langle |C(f)|^2\rangle_m \tag{8}$$

where C is the T-M noise PSD of the device under test, which is the value of interest. Such partially correlated signals are encountered in a situation where a single output of the device under test (*e.g.*, a RCA CMUT array) is divided into two channels. An illustration of this measurement protocol is presented Fig. 11.

Note that the key point for the cross-spectrum method to be applied, is to perform the acquisition of signals $x(t)$ and $y(t)$ at the same time to ensure that the noise $c(t)$ is correlated between the two signals.

To illustrate the differences between the two approaches, the noise generated by a 50 Ω purely resistive load was measured using the temporal setup (cf. next paragraph). The signal was divided into two 50 Ω RG-58 coaxial cables of 10 *cm* each and connected to two different oscilloscope channels with matched impedance. Post-processing based on auto- and a cross-correlation was applied over $m = 256$ aquisitions, and results are presented Fig. 12.

Using cross-correlation, the global noise is greatly reduced towards the theoretical noise voltage value. As expected, the uncorrelated noise originating from the acquisition channels vanishes. The preferred temporal approach for the remaining measurements in this paper is therefore the cross-correlation approach. If the signal generated by the device of interest is superior to either one of those noise floors, both the auto- and the cross-correlation approaches are suitable.

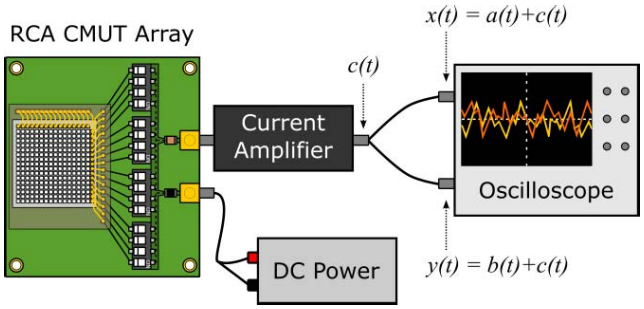

FIGURE 11. Experimental principle behind the cross-spectrum method applied to a current driven DC powered RCA CMUT array integrated on a PCB. The oscilloscope requires at least two channel inputs that both contains the noise from the device under test and uncorrelated noise sources.

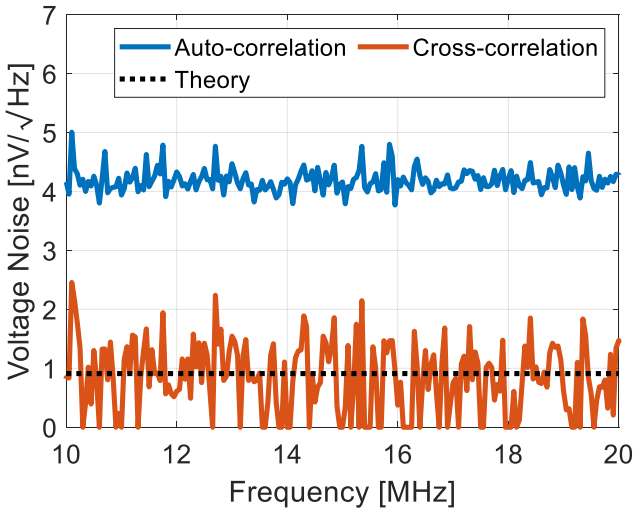

FIGURE 12. Temporal voltage noise measurements of a 50 Ω resistive load post-processed using the auto- and cross-correlation approaches and compared with its theoretical value.

B. RESULTS AND DISCUSSION

Temporal measurements were performed with a 12 bits HDO6034A oscilloscope (TeledyneLecroy, Chestnut Ridge, NY, USA). Frequency domain measurements were performed using the N9010A signal analyzer, which is usually the "go-to" type of platform for T-M noise assessment. CMUT biasing voltage was delivered by a DC power supply (PLHP250-P, Aim & Thurlby Thandar Instruments Ltd., Huntingdon, Cambridgeshire, UK) and a standard 50Ω RG-58 coaxial cable was used to connect the different devices with matched impedances. No external source was applied. The two different setups are presented Fig. 13.

Using the temporal approach, results were obtained with 256 different acquisitions, no averaging, and a sampling frequency of 500 *MHz*. Using the frequential method, the spectrum analyzer parameters were set to a RBW of 30 *kHz* and a video bandwidth (VBW) of 10 *Hz*. Measurements with both methods had a similar acquisition time of about one minute. The results obtained for different bias voltages on

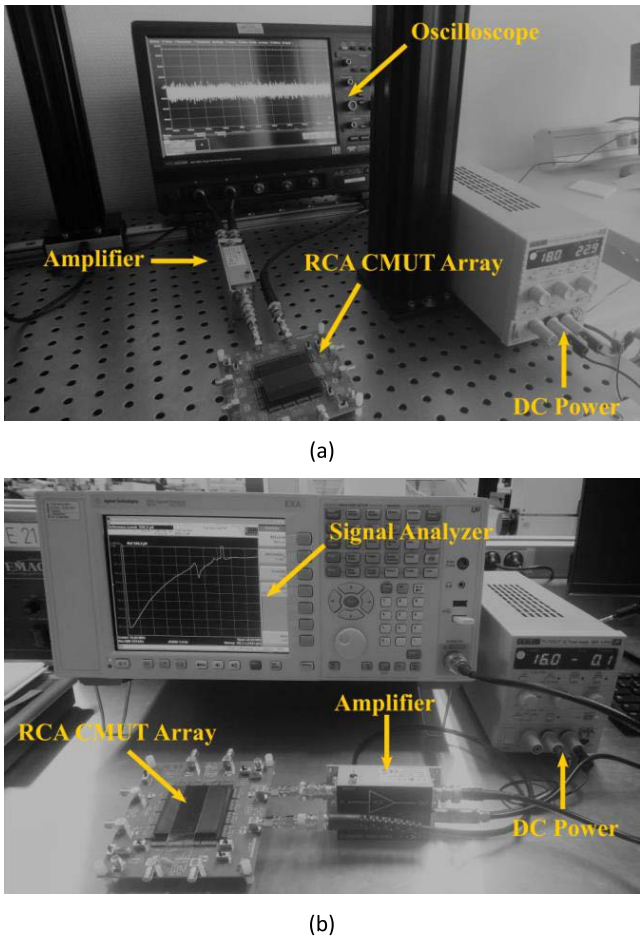

FIGURE 13. **Photos of (a) the temporal setup where the output of the amplifier is connected to two oscilloscope inputs and (b) the frequential setup using a single channel signal analyzer.**

a RCA element are compared with the modeling approach described Section III of this paper and are presented Fig. 14.

Both experimental methods give almost identical results and demonstrate that they can be used to assess T-M noise in good general agreement with the model. The results are in accordance with the electrical admittance previously measured of the bare dice (cf. Fig. 5). Indeed, the parasitic components of the characterization PCB are translated though the amplifier and appear on the noise measurements for frequencies higher than the anti-resonance. Nevertheless, this shows that the proposed temporal method employed on a digital oscilloscope and combined with cross-spectrum post-processing can be used to assess T-M noise accurately using a general-purpose commercially available amplifier.

As intended, noise characterization enabled the evaluation of the overall performance, collapse voltage and working frequencies of this air coupled RCA CMUT device fabricated. According to the bias voltage value, the spring softening effect is observed, the resonance decreases, and the overall noise amplitude increases. Note that only raw data were presented, no normalization, smoothing or filtering was applied. Increasing the signal analyzer RBW and the number of oscilloscope acquisitions may improve the overall results precision.

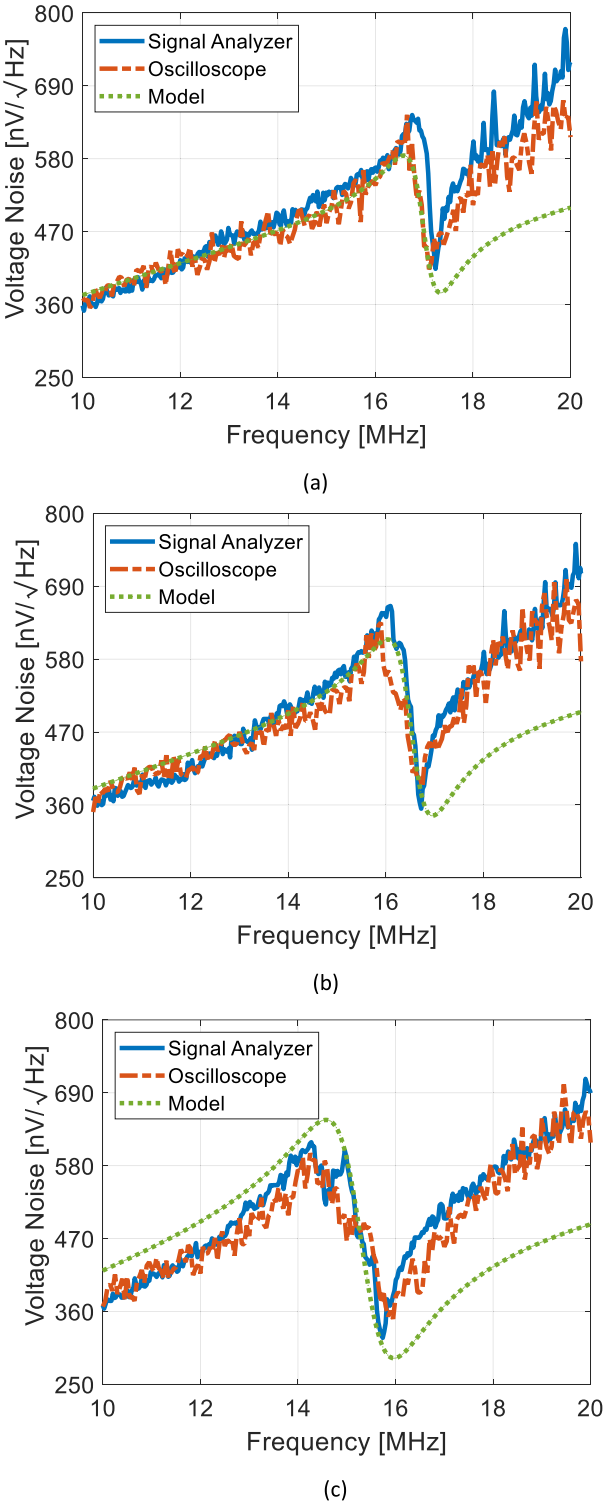

FIGURE 14. **Measurements and modeling of the voltage noise of a RCA CMUT probe element as a function of frequency using the temporal method on a digital oscilloscope and the frequential method on a signal analyzer. The results are obtained for (a) $V_{DC} = 0.6V_C$, (b) $V_{DC} = 0.7V_C$ and (c) $V_{DC} = 0.85V_C$.**

V. CONCLUSION

T-M noise is an important characteristic of MEMS transducers but previously remained a difficult task with little to no successful generalization of a measurement protocol easily applicable to different systems. In this paper, we focused our efforts on a low impedance current driven row-column addressed capacitive micromachined transducer array designed for ultrasound imaging and used as two orthogonal 1-D linear arrays. A lumped-parameter modeling approach was proposed with cascaded two port networks to simulate the T-M noise PSD of a full instrumentation chain. We proposed two characterization protocols using a commercially available current amplifier. A temporal method was used through a digital oscilloscope with a post processing step that takes advantage of signal cross-correlation properties. A frequency domain method was also employed using a spectrum analyzer for comparison. Measurements are in great agreement between one another. These methods are also applicable to other technologies (*e.g.*, PMUT arrays), architectures and amplifiers. No external source and calibration process was needed. The parasitic components of the CMUT array element were shown to influence the T-M noise. The characteristics of the amplifier allowed us to model a complete measurement chain with great accuracy regarding measurement results. This work was focused on an air coupled RCA CMUT probe and we presented T-M noise properties of such devices using a dedicated PCB that can still be improved. Future works will aim to use this method on other technologies, array architectures and fluid coupled microsystems.

APPENDIX

PRINCIPLE BEHIND THE CROSS-SPECTRUM METHOD

Let us consider two signals $x(t)$ and $y(t)$ comprised of two uncorrelated parasitic noise sources $a(t)$ and $b(t)$ and one correlated noise source $c(t)$ such that

$$\begin{cases} x\,(t) = a\,(t) + c(t) \\ y\,(t) = b\,(t) + c\,(t) \end{cases} \tag{9}$$

Here, $c\,(t)$ is the noise directly related to the device under test, hence the value of interest. The mean Cross Power Spectral Density (CPSD) $\langle S_{xy}\rangle$ evaluation of equation (9) over a number of m spectra leads to

$$\begin{aligned} \left\langle S_{xy}\,(f)\right\rangle_m &= \frac{1}{T}\left\langle X^*\,(f)\,Y\,(f)\right\rangle_m \\ \left\langle S_{xy}\,(f)\right\rangle_m &= \frac{1}{T}\left\langle [A\,(f) + C\,(f)]^*\,[B\,(f) + C\,(f)]\right\rangle_m \end{aligned} \tag{10}$$

This result can be further developed to get the complete expression of the CPSD such that

$$\begin{aligned} \left\langle S_{xy}\,(f)\right\rangle_m = \frac{1}{T}\Big[&\left\langle A\,(f)^*\,B\,(f)\right\rangle_m + \left\langle A\,(f)^*\,C\,(f)\right\rangle_m \\ &+ \left\langle C\,(f)^*\,B\,(f)\right\rangle_m \\ &+ \left\langle C\,(f)^*\,C\,(f)\right\rangle_m\Big] \end{aligned} \tag{11}$$

Theoretically, the multiplication of two uncorrelated noise spectra averaged over a large enough number m tends towards zero. Hence, the first three terms of equation (11) vanish and one gets

$$\langle S_{xy}(f)\rangle_m = \frac{1}{T}\langle C(f)^* C(f)\rangle_m = \frac{1}{T}\langle |C(f)|^2\rangle_m \tag{12}$$

which is the noise PSD of the device under test, hence the value of interest. The cross-spectrum technique has been thoroughly described in great details by Rubiola and Vernotte [17]. Note that there are statistical limits to this approach [36] and if not properly addressed, phase inversion of correlated signals may result in the method collapse [37].

ACKNOWLEDGMENT

The authors would like to thank Edgard Jeanne for the CMUT array design and Sébastien Augier for the device integration.

REFERENCES

[1] J. B. Johnson, "Thermal agitation of electricity in conductors," *Phys. Rev.*, vol. 32, pp. 97–109, Jul. 1928.
[2] H. Nyquist, "Thermal agitation of electric charge in conductors," *Phys. Rev.*, vol. 32, no. 1, pp. 110–113, Jul. 1928.
[3] F. Mohd-Yasin, D. J. Nagel, and C. E. Korman, "Noise in MEMS," *Meas. Sci. Technol.*, vol. 21, no. 1, Jan. 2010, Art. no. 012001.
[4] S. C. Thompson *et al.*, "Noise in miniature microphones," *J. Acoust. Soc. Amer.*, vol. 111, no. 2, pp. 861–866, Feb. 2002.
[5] T. B. Gabrielson, "Mechanical-thermal noise in micromachined acoustic and vibration sensors," *IEEE Trans. Electron Devices*, vol. 40, no. 5, pp. 903–909, May 1993.
[6] Y. M. Blanter and M. Büttiker, "Shot noise in mesoscopic conductors," *Phys. Rep.*, vol. 336, nos. 1–2, pp. 1–166, Sep. 2000.
[7] K. K. Hung, P. K. Ko, C. Hu, and Y. C. Cheng, "A unified model for the flicker noise in metal-oxide-semiconductor field-effect transistors," *IEEE Trans. Electron Devices*, vol. 37, no. 3, pp. 654–665, Mar. 1990.
[8] G. Gurun, M. Hochman, P. Hasler, and F. L. Degertekin, "Thermal-mechanical-noise-based CMUT characterization and sensing," *IEEE Trans. Ultrason., Ferroelectr., Freq. Control*, vol. 59, no. 6, pp. 1267–1275, Jun. 2012.
[9] D. W. Schindel, D. A. Hutchins, L. Zou, and M. Sayer, "The design and characterization of micromachined air-coupled capacitance transducers," *IEEE Trans. Ultrason., Ferroelectr., Freq. Control*, vol. 42, no. 1, pp. 42–50, Jan. 1995.
[10] M. I. Haller and B. T. Khuri-Yakub, "A surface micromachined electrostatic ultrasonic air transducer," *IEEE Trans. Ultrason., Ferroelectr., Freq. Control*, vol. 43, no. 1, pp. 1–6, Jan. 1996.
[11] J. Joseph, B. Ma, and B. T. Khuri-Yakub, "Applications of capacitive micromachined ultrasonic transducers: A comprehensive review," *IEEE Trans. Ultrason., Ferroelectr., Freq. Control*, vol. 69, no. 2, pp. 456–467, Feb. 2022.
[12] I. O. Wygant, M. Kupnik, and B. T. Khuri-Yakub, "CMUT design equations for optimizing noise figure and source pressure," in *Proc. IEEE Int. Ultrason. Symp. (IUS)*, Sep. 2016, pp. 1–4.
[13] A. Bozkurt and G. G. Yaralioglu, "Receive-noise analysis of capacitive micromachined ultrasonic transducers," *IEEE Trans. Ultrason., Ferroelectr., Freq. Control*, vol. 63, no. 11, pp. 1980–1987, Nov. 2016.
[14] B.-H. Kim and H.-S. Lee, "Acoustical-thermal noise in a capacitive MEMS microphone," *IEEE Sensors J.*, vol. 15, no. 12, pp. 6853–6860, Dec. 2015.
[15] G. Gurun, P. Hasler, and F. L. Degertekin, "Front-end receiver electronics for high-frequency monolithic CMUT-on-CMOS imaging arrays," *IEEE Trans. Ultrason., Ferroelectr., Freq. Control*, vol. 58, no. 8, pp. 1658–1668, Aug. 2011.
[16] I. O. Wygant *et al.*, "Integration of 2D CMUT arrays with front-end electronics for volumetric ultrasound imaging," *IEEE Trans. Ultrason., Ferroelectr., Freq. Control*, vol. 55, no. 2, pp. 327–342, Feb. 2008.
[17] E. Rubiola and F. Vernotte, "The cross-spectrum experimental method," 2010, *arXiv:1003.0113*.
[18] P. Roux, K. G. Sabra, P. Gerstoft, W. A. Kuperman, and M. C. Fehler, "P-waves from cross-correlation of seismic noise," *Geophys. Res. Lett.*, vol. 32, no. 19, pp. 1–4, 2005.

[19] A. Bertolo, J. Sauvage, M. Tanter, M. Pernot, and T. Deffieux, "XDoppler: Cross-correlation of orthogonal apertures for 3D blood flow imaging," *IEEE Trans. Med. Imag.*, vol. 40, no. 12, pp. 3358–3368, Dec. 2021.
[20] P. Wagner, C. Daft, S. Panda, and I. Ladabaum, "Two approaches to electronically scanned 3D imaging using cMUTs," in *Proc. IEEE Ultrason. Symp.*, vol. 1, Oct. 2006, pp. 685–688.
[21] A. S. Erguri, Y. Huang, X. Zhuang, Ö. Oralkan, G. G. Yarahoglu, and B. T. Khuri-Yakub, "Capacitive micromachined ultrasonic transducers: Fabrication technology," *IEEE Trans. Ultrason., Ferroelectr., Freq. Control*, vol. 52, no. 12, pp. 2242–2258, Dec. 2005.
[22] J. L. Sanders, A. O. Biliroglu, X. Wu, O. J. Adelegan, F. Y. Yamaner, and Ö. Oralkan, "A row-column (RC) addressed 2-D capacitive micromachined ultrasonic transducer (CMUT) array on a glass substrate," *IEEE Trans. Ultrason., Ferroelectr., Freq. Control*, vol. 68, no. 3, pp. 767–776, Mar. 2021.
[23] A. Sampaleanu, P. Zhang, A. Kshirsagar, W. Moussa, and R. J. Zemp, "Top-orthogonal-to-bottom-electrode (TOBE) CMUT arrays for 3-D ultrasound imaging," *IEEE Trans. Ultrason., Ferroelectr., Freq. Control*, vol. 61, no. 2, pp. 266–276, Feb. 2014.
[24] M. Schou *et al.*, "Fast 3-D velocity estimation in 4-D using a 62 + 62 row–column addressed array," *IEEE Trans. Ultrason., Ferroelectr., Freq. Control*, vol. 68, no. 3, pp. 608–623, Mar. 2021.
[25] S. Krusevac, P. B. Rapajic, and R. A. Kennedy, "Mutual coupling effect on thermal noise in multi-element antenna systems," in *Proc. Prog. Electromagn. Res. Symp. (PIERS)*, 2005, pp. 53–57.
[26] T. Merrien, A. Boulme, and D. Certon, "Lumped-parameter equivalent circuit modeling of CMUT array elements," *IEEE Open J. Ultrason., Ferroelectr., Freq. Control*, vol. 2, pp. 1–16, 2022.
[27] C. Meynier, F. Teston, and D. Certon, "A multiscale model for array of capacitive micromachined ultrasonic transducers," *J. Acoust. Soc. Amer.*, vol. 128, no. 5, pp. 2549–2561, 2010.
[28] D. Certon, F. Teston, and F. Patat, "A finite difference model for cMUT devices," *IEEE Trans. Ultrason., Ferroelectr., Freq. Control*, vol. 52, no. 12, pp. 2199–2210, Dec. 2005.
[29] A. Unlugedik, A. S. Taşdelen, A. Atalar, and H. Köymen, "Designing transmitting CMUT cells for airborne applications," *IEEE Trans. Ultrason., Ferroelectr., Freq. Control*, vol. 61, no. 11, pp. 1899–1910, Nov. 2014.
[30] M. Khan, T. M. Khan, A. S. Tasdelen, M. Yilmaz, A. Atalar, and H. Koymen, "Optimization of a collapsed mode CMUT receiver for maximum off-resonance sensitivity," *J. Microelectromech. Syst.*, vol. 27, no. 5, pp. 921–930, Oct. 2018.
[31] A. S. Havreland, M. Engholm, B. G. Tomov, J. A. Jensen, O. Hansen, and E. V. Thomsen, "CMUT electrode resistance design: Modeling and experimental verification by a row–column array," *IEEE Trans. Ultrason., Ferroelectr., Freq. Control*, vol. 66, no. 6, pp. 1110–1118, Jun. 2019.
[32] M. Engholm *et al.*, "Probe development of CMUT and PZT row–column-addressed 2-D arrays," *Sens. Actuators A, Phys.*, vol. 273, pp. 121–133, Apr. 2018.
[33] H. B. Callen and T. A. Welton, "Irreversibility and generalized noise," *Phys. Rev.*, vol. 83, no. 1, pp. 34–40, Jul. 1951.
[34] T. L. Rhyne, "Characterizing ultrasonic transducers using radiation efficiency and reception noise figure," *IEEE Trans. Ultrason., Ferroelectr., Freq. Control*, vol. 45, no. 3, pp. 559–566, May 1998.
[35] R. Krishnakumar and R. Ramesh, "A method and an experimental setup for measuring the self-noise of piezoelectric hydrophones," *IEEE Trans. Ultrason., Ferroelectr., Freq. Control*, vol. 67, no. 2, pp. 413–421, Feb. 2020.
[36] A. Baudiquez, E. Lantz, E. Rubiola, and F. Vernotte, "Cross-spectrum measurement statistics: Uncertainties and detection limit," *IEEE Trans. Ultrason., Ferroelectr., Freq. Control*, vol. 67, no. 11, pp. 2461–2470, Nov. 2020.
[37] C. W. Nelson, A. Hati, and D. A. Howe, "A collapse of the cross-spectral function in phase noise metrology," *Rev. Sci. Instrum.*, vol. 85, no. 3, Feb. 2014, Art. no. 024705.

TONY MERRIEN was born in Rennes, France, in 1994. He received the M.Sc. degree in physical acoustics from the École Centrale de Lyon, France, in 2018. He is currently pursuing the Ph.D. degree in electrical engineering with the GREMAN UMR-CNRS 7347 Laboratory, in partnership with MODULEUS SAS. His current research focuses on row-column addressed (RCA) capacitive micromachined ultrasonic transducers (CMUT) integration for 3D imaging.

AUDREN BOULMÉ was born in France, in 1987. He received the M.Sc. degree in medical imaging technology from the François Rabelais University of Tours, France, in 2009, and the Ph.D. degree in engineering physics from the University of Tours, France, in 2013. In 2017, he joined MODULEUS SAS as a Research and Development Engineer. His research focuses on modeling, design, and characterization of capacitive micromachined ultrasonic transducers (CMUT).

DOMINIQUE CERTON (Member, IEEE) received the M.Sc. degree in signal processing and electrical engineering from the University of Orléans, France, in 1991, and the Ph.D. and Habilitation à Diriger des Recherches (HDR) degrees in applied acoustics and materials engineering from the University of Tours, France, in 1994 and 2006, respectively. He is currently a Full Professor affiliated with the GREMAN Laboratory (UMR-CNRS 7347—University of Tours). In addition to his research activities, he is in charge of coordinating the Electronics and Energy Department, Polytech Tours Engineering School. For more than ten years, he has developed strong know-how in the design, modeling, and characterization of MEMS-based ultrasonic transducers, i.e., capacitive micromachined ultrasonic transducers (CMUT). He also has over ten years of research experience with multi-element probes based on piezoelectric materials and more specifically with piezo-composite materials. He has been involved in several national and international research projects and has coordinated national research projects funded by the French National Research Agency. A large part of his activities has led to strong industrial collaborations and the transfer of know-how. This relationship with industrial partners has enabled the development, use, and exploitation of tools for modeling multi-element ultrasound probes. He has authored or coauthored more than 60 communications and publications. His research activities focus on ultrasonic probes, instrumentation applied to medical imaging, nondestructive testing, and metrology. He is a member of the French Society of Acoustics.